EUROPEAN ORGANIZATION FOR NUCLEAR RESEARCH

ALICE-ANA-2014-xxx
May 4, 2020

Analysis of light vector mesons in p–p collisions at $\sqrt{s} = 13$ TeV

Jonathan Kley[1]

1. Technical University of Munich

Email: jonathan.kley@cern.ch

Abstract

Here goes your abstract

Contents

1 Introduction[1]

With the exploration of the phase diagram of nuclear matter has come the idea of the Quark gluon plasma (QGP), a state of matter where confinement is abolished and quarks and gluons can move quasi-freely. However, they still interact strongly, so the medium behaves more like a perfect liquid than a gas. The QGP is created when a critical temperature of $T_c = (154 \pm 9)$ MeV is exceeded [2]. In the laboratory heavy ion collisions are used to deposit a lot of energy in a small spatial volume making it possible to exceed the critical temperature and creating a QGP. After thorough theoretical investigations, experiments in the late 80s started looking for the QGP, but definite traces where only found in the early 2000s by the RHIC experiments at Brookhaven National Laboratory [3]. Since then other experiments also joined in on the search for the QGP. After the SPS experiments at CERN could not find any traces of the formation of a QGP, CERN built a dedicated LHC experiment to investigate heavy ion collisions and the QGP, the ALICE experiment [4] which was also used to obtain the data which is analysed here. Because of the short life time (of $O(10\frac{fm}{c})$ [5]) of the QGP and its strongly interacting nature, it is very difficult to gain information about the properties of the QGP. This is mainly because particles either live too long to decay inside the QGP and therefore lose their information. Or if they decay inside the QGP, their decay products might interact strongly and lose the information they carry about the QGP through scattering in the QGP. So, the most important probes to investigate the QGP are short-lived particles which decay into particles which only interact electromagnetically. One candidate are vector mesons which carry the same quantum numbers as photons ($J^P = 1^-$) and couple to them (and therefore effectively to dileptons) as explained by the vector-dominance model. The dileptons are a very clean experimental probe and can be identified with high precision in the ALICE TPC.

One of the most interesting aspects of the QGP is the possible restoration of the chiral symmetry which might also be connected to a phase transition in the phase diagram of nuclear matter. There are many implications of this possible restoration of chiral symmetry on the particle spectrum of QCD which in reverse can also be used to check if our fundamental theory of the strong interaction – QCD – is correct. One system which should in theory be affected by the restoration of chiral symmetry and also is the ρ-a_1 system. If chiral symmetry is present these two particles are related to each other which has consequences on their so-called spectral functions.

This work is a feasibility study of the measurement of the a_1 meson at the ALICE experiment in pp collisions. Along the a_1 meson we also try to identify vector mesons which appear in the same decay channels to double check our results.

This paper is structured as follows. In section 1 I will discuss the chiral symmetry of QCD and its consequences in more detail, also including implications on the ρ-a_1 system. I will then discuss the details of the data analysis in section 2 including the analysis strategy and particle cuts and event selection. Finally in section 3, I will discuss the results and give a quick outlook in section 4.

1.1 The QCD Lagrangian

To understand the effects of the strong interaction we use the theory which has been proven most successful in this matter in the end of the last century: QCD. We start from the classic Lagrangian of QCD with 3 flavours which is the unique Lagrangian which is invariant under a gauged SU(3) symmetry

$$\mathscr{L}_{QCD} = \bar{\psi}_i \left(i\gamma_\mu D^\mu - m\right)_{ij} \psi_j - \frac{1}{4} G^a_{\mu\nu} G^{\mu\nu}_a \tag{1}$$

[1] The introduction is mostly based on [1] with other references used where cited.

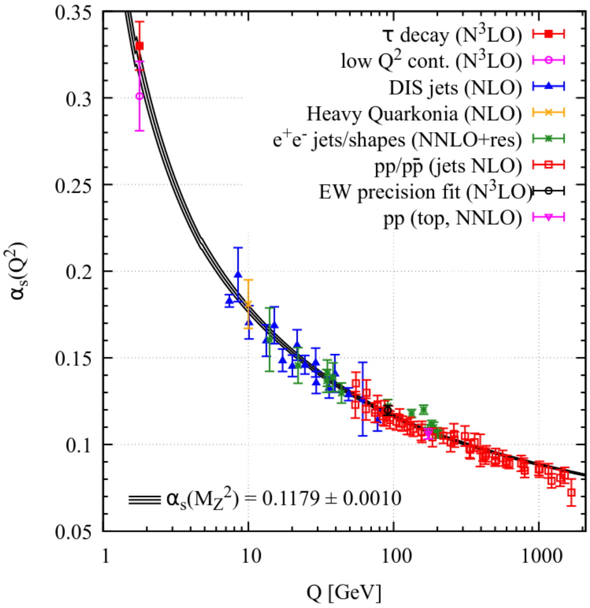

Fig. 1: The running coupling of QCD [7]. Summary of measurements of α_S as a function of the scale Q. The order in QCD perturbation theory which was used in the calculation is indicated in brackets.

where $\psi = (u,d,s)$ are the quark fields, $D^\mu = \partial^\mu - igA^\mu$ is the covariant derivative in the fundamental representation and $G^a_{\mu\nu} = \partial_\mu A_\nu - \partial_\nu A_\mu + gf^{abc}A^b_\mu A^c_\nu$ is the field strength of the gluon fields A^a_μ with the structure constants f^{abc} of SU(3).
Following the usual procedure of perturbative renormalization we can calculate the β-function in QCD. At 1-loop order it is given by [6]

$$\beta(\alpha_S) = \mu_R^2 \frac{d\alpha_S}{d\mu_R^2} = -\left(11 - \frac{2}{3}n_f\right)\frac{\alpha_S^2}{4\pi} + O(\alpha_S^3) \equiv -\beta_0 \frac{\alpha_S^2}{4\pi} + O(\alpha_S^3) \tag{2}$$

where n_f is the number of flavours and β_0 the 1-loop β-function coefficient. Solving the differential equation in eqn. 2 in terms of the renormalized scale μ_R^2 we get an expression for the running coupling in QCD. Using the 1-loop expression we get

$$\alpha_S(\mu) = \frac{4\pi}{\beta_0 \log \frac{\mu^2}{\Lambda^2}} \tag{3}$$

where Λ is the QCD scale and we fixed $\alpha(\mu) \xrightarrow{\mu\to\Lambda} \infty$. A plot of the running coupling along with the most recent measurements can be seen in fig. 1.
From eqn. 3 it is obvious that perturbation theory is not applicable at energy scales close to the fundamental scale of our theory. Unfortunately this is the regime we are interested in, so we have to think of another way to approach scales $\mu < \Lambda_{QCD}$.

1.2 Chiral Symmetry of QCD

One of the ways to approach regimes where $\mu < \Lambda_{QCD}$ is to build an effective Lagrangian based on the symmetries of the fundamental Lagrangian of QCD. In this section we investigate this approach and see which implications it has for the particle spectrum of the theory.
We start from the Lagrangian of QCD in eqn. 1. Of particular interest to us for the chiral symmetry is the quark term in the Lagrangian which can be split into two parts

$$\mathscr{L}_{\text{quarks}} = \bar{\psi} i\gamma_\mu D^\mu \psi - m\bar{\psi}\psi \equiv \mathscr{L} + \delta\mathscr{L} \tag{4}$$

The suggestive names will make sense in a second. Since the doublet of quark fields in $\mathscr{L}$ are contracted in an inner product the Lagrangian is invariant under an inner symmetry. In our case this is a U(2) symmetry for both chiralities, so $U(2)_L\times U(2)_R$ in total. We can also think of the symmetries in terms of axial and vector currents instead of left and right handed currents which is more useful in this analysis, so the symmetry group is $U(2)_V\times U(2)_A$. We only consider the SU(2) part of both subgroups, since $U(1)_V$ can be identified with baryon number conservation and $U(1)_A$ is anomalous because th, so it is not a real symmetry of our theory. Let us consider the following SU(2) transformations

$$U_V = \exp\left(-i\alpha^i\frac{\sigma^i}{2}\right) \approx 1 - i\alpha^i\frac{\sigma^i}{2} \in SU(2)_V \tag{5}$$

$$U_A = \exp\left(-i\gamma_5\alpha^i\frac{\sigma^i}{2}\right) \approx 1 - i\gamma_5\alpha^i\frac{\sigma^i}{2} \in SU(2)_A \tag{6}$$

of the quark fields and their action on $\mathscr{L}$

$$\mathscr{L} = i\psi^\dagger\gamma_0\gamma^\mu D_\mu\psi \xrightarrow{U_V} i\left(U_V\psi\right)^\dagger\gamma_0\gamma^\mu D_\mu U_V\psi = i\psi^\dagger e^{+i\alpha^i\frac{\sigma^i}{2}}\gamma_0\gamma^\mu D_\mu e^{-i\alpha^i\frac{\sigma^i}{2}}\psi = i\bar{\psi}\not{D}\psi \tag{7}$$

and

$$\mathscr{L} = i\psi^\dagger\gamma_0\gamma^\mu D_\mu\psi \xrightarrow{U_A} i\left(U_A\psi\right)^\dagger\gamma_0\gamma^\mu D_\mu U_A\psi = i\psi^\dagger e^{+i\alpha^i\gamma_5\frac{\sigma^i}{2}}\gamma_0\gamma^\mu D_\mu e^{-i\gamma_5\alpha^i\frac{\sigma^i}{2}}\psi = i\bar{\psi}\not{D}\psi \tag{8}$$

where we used $\{\gamma^\mu,\gamma_5\} = 0 = [D^\mu,\gamma_5]$ and $\gamma_5^\dagger = \gamma_5$. So $\mathscr{L}$ is invariant under both U_V and U_A. The corresponding currents are

$$j^i_\mu = \bar{\psi}\gamma_\mu\frac{\sigma^i}{2}\psi \tag{9}$$

$$j^i_{5\mu} = \bar{\psi}\gamma_\mu\gamma_5\frac{\sigma^i}{2}\psi \tag{10}$$

Now we can check the effect of the transformations on $\delta\mathscr{L}$

$$\delta\mathscr{L} = -m\psi^\dagger\gamma^0\psi \xrightarrow{U_V} -m\left(U_V\psi\right)^\dagger\gamma^0 U_V\psi = -m\psi^\dagger e^{+i\alpha^i\frac{\sigma^i}{2}}\gamma^0 e^{-i\alpha^i\frac{\sigma^i}{2}}\psi = -m\bar{\psi}\psi \tag{11}$$

and

$$\delta\mathscr{L} = -m\psi^\dagger\gamma^0\psi \xrightarrow{U_A} -m\left(U_A\psi\right)^\dagger\gamma^0 U_A\psi = -m\psi^\dagger e^{+i\gamma_5\alpha^i\frac{\sigma^i}{2}}\gamma^0 e^{-i\gamma_5\alpha^i\frac{\sigma^i}{2}}\psi = -me^{2i\gamma_5\alpha^i\frac{\sigma^i}{2}}\bar{\psi}\psi \neq \delta\mathscr{L} \tag{12}$$

where we used the same identities as above. We see that the mass term is not invariant under axial transformations while it is left invariant by vector transformations. The axial symmetry is therefore explicitly broken by the quark mass term. But as long as the quark masses are smaller than the scale of our theory we can still use the symmetry as an approximate symmetry. This is indeed the case, since $m_u, m_d \sim O(5\text{ MeV}) \ll \Lambda_{QCD} \simeq 200\text{ MeV}$.

1.3 Spontaneous Chiral Symmetry Breaking

With our 2 quark fields we can now build bosonic fields that have the quantum numbers of the mesons in nature. We find

$$\begin{aligned} &\text{pion}-\text{like state}: \vec{\pi} \equiv i\bar{\psi}\vec{\sigma}\gamma_5\psi; && \text{sigma}-\text{like state}: \sigma \equiv \bar{\psi}\psi \\ &\text{rho}-\text{like state}: \vec{\rho}_\mu \equiv \bar{\psi}\vec{\sigma}\gamma_\mu\psi; && a_1-\text{like state}: \vec{a}_{1\mu} \equiv \bar{\psi}\vec{\sigma}\gamma_\mu\gamma_5\psi \end{aligned}$$

Of particular interest to us will be the ρ and the a_1 states because they correspond to the conserved currents from eqn. 9 and 10 and therefore seem to be closely related to the chiral symmetry. Let us see now how these particles transform under the chiral transformations in infinitesimal form, so we can understand the symmetry better. Starting with the π state and with the vector transformation from eqn. 5 we get

$$i\bar{\psi}\sigma^i\gamma_5\psi \xrightarrow{U_V} i\left(U_V\psi\right)^\dagger\gamma^0\sigma^i\gamma_5U_V\psi = i\bar{\psi}\sigma^i\gamma_5\psi + \alpha^j\left(\bar{\psi}\sigma^i\frac{\sigma^j}{2}\gamma_5\psi - \bar{\psi}\frac{\sigma^j}{2}\sigma^i\gamma_5\psi\right) + O(\alpha^2) =$$
$$= i\bar{\psi}\sigma^i\gamma_5\psi + i\alpha^j\varepsilon^{ijk}\bar{\psi}\sigma^k\gamma_5\psi \tag{13}$$

where we have used the $SU(2)$ algebra $\left[\sigma^i,\sigma^j\right] = 2i\varepsilon^{ijk}\sigma^k$. We can do similar calculations for all of the other states as well and get for the vector transformations

$$\vec{\pi} \xrightarrow{U_V} \vec{\pi} + \vec{\alpha}\times\vec{\pi} \tag{14}$$
$$\sigma \xrightarrow{U_V} \sigma \tag{15}$$
$$\vec{\rho}_\mu \xrightarrow{U_V} \vec{\rho}_\mu + \vec{\alpha}\times\vec{\rho}_\mu \tag{16}$$
$$\vec{a}_{1\mu} \xrightarrow{U_V} \vec{a}_{1\mu} + \vec{\alpha}\times\vec{a}_{1\mu} \tag{17}$$

Which is also what we expect when we identify $SU(2)_V$ with isospin. $\vec{\pi}$, $\vec{\rho}_\mu$ and $\vec{a}_{1\mu}$ are all in the fundamental representation of isospin and are therefore changed by an isospin rotation. Whereas, σ is a scalar under isospin and is therefore not affected.
However, under the axial transformations the particles mix as follows

$$\vec{\pi} \xrightarrow{U_A} \vec{\pi} + \vec{\alpha}\sigma \tag{18}$$
$$\sigma \xrightarrow{U_A} \sigma - \vec{\alpha}\cdot\vec{\pi} \tag{19}$$
$$\vec{\rho}_\mu \xrightarrow{U_A} \vec{\rho}_\mu + \vec{\alpha}\times\vec{a}_{1\mu} \tag{20}$$
$$\vec{a}_{1\mu} \xrightarrow{U_A} \vec{a}_{1\mu} - \vec{\alpha}\times\vec{\rho}_\mu \tag{21}$$

Since 2 pairs of particles are rotated into each other by axial rotations, this suggests that these particles have the same mass or after the explicit breaking of $SU(2)_A$ by the quark mass term at least a similar mass. But this does not seem to be the case in nature, since e.g. the a_1 has a mass of $m_{a_1} \simeq 1260$ MeV which is almost double the mass of the ρ meson with a mass of $m_\rho \simeq 770$ MeV.
So, clearly $m_{a_1} \not\simeq m_\rho$ and $SU(2)_A$ can not be a symmetry of the vacuum and must therefore be spontaneously broken: $SU(2)_V \times SU(2)_A \to SU(2)_V$. This can also be seen from the vacuum expectation value (VEV) of the term $\bar{\psi}\psi$

$$\langle 0|\bar{\psi}\psi|0\rangle \xrightarrow{U_A} \langle 0|\bar{\psi}e^{-2i\gamma_5\alpha^i\frac{\sigma^i}{2}}\psi|0\rangle \tag{22}$$

which would be invariant if the vacuum was invariant: $U_A|0\rangle = e^{-i\gamma_5\alpha^i\frac{\sigma^i}{2}}|0\rangle = |0\rangle$. However, this is not the case in nature as we just discussed. Therefore, $SU(2)_A$ must be spontaneously broken and $\bar{\psi}\psi$ – the so-called chiral condensate – must develop a vacuum expectation value $\langle\bar{\psi}\psi\rangle = -(250\text{MeV})^3$. We can use the VEV as an order parameter for the breaking of $SU(2)_A$. If the symmetry is not broken the VEV is zero and if we have a finite VEV the symmetry is broken as we expect from an order parameter.
We can now interpret the three spin-0 particles $\vec{\pi}$ from above as the Goldstone bosons of the spontaneously broken $SU(2)_A$. If $U(1)_A$ wasn't anomalous, we could identify the σ as its Goldstone boson, which in the case of three flavours can be identified with the η'.
We could now turn on the usual machinery for spontaneously broken symmetries and construct the effective Lagrangian of the pions. But since we don't do any original calculations in this paper, let us skip that and look at some implications of the spontaneous symmetry breaking and the possible return of the symmetry. Especially in the for the vector mesons whose field configurations correspond to the conserved currents.

1.4 Effects of Hot Matter on Chiral Symmetry

In this section I want to discuss the possible effects of hot and dense matter – like a QGP – on observables. In our case only the temperature dependence is interesting, since the ALICE experiment operates at zero baryon chemical potential. The QGP in ALICE is created by depositing as much energy as possible in a small spatial volume and then hoping to reach a temperature $T > T_c$.
Let us start with the discussion of the order parameter of chiral symmetry which we just defined in eqn. 22. Gerber and Leutwyler showed that up to 3-loop order the temperature dependence of $\langle\bar{\psi}\psi\rangle$ for $T < T_c$ and massless quarks is given by [8]

$$\frac{\langle\bar{\psi}\psi\rangle(T)}{\langle\bar{\psi}\psi\rangle(T=0)} = 1 - x - \frac{1}{6}x^2 - \frac{16}{9}x^3 \ln\frac{T}{\Lambda_q} \tag{23}$$

where $x = \frac{T^2}{8f^2}$, the relevant temperature scale is $\sqrt{8}f \simeq 250$ MeV with f the pion decay constant in the chiral limit and $\Lambda_q = (470 \pm 110)$ MeV. We can see a clear trend of a decreasing order parameter for increasing temperature which suggests a restoration of chiral symmetry if the trend continues.
The temperature dependence over a bigger interval can be obtained from lattice QCD. The results of one such calculation can be found in fig. 2. Here we can see that the trend indeed continues and chiral symmetry seems to be restored in a QGP. This of course has consequences on the things we discussed earlier.
Let us define the following correlators

$$\Pi^{VV}_{\mu\nu}(q) = i\int d^4x e^{iq\cdot x}\langle 0|\mathscr{T} j^V_\mu(x) j^V_\nu(0)|0\rangle = \left(-q^2 g_{\mu\nu} + q_\mu q_\nu\right)\Pi_V(q^2) \tag{24}$$

and

$$\Pi^{AA}_{\mu\nu}(q) = i\int d^4x e^{iq\cdot x}\langle 0|\mathscr{T} j^A_\mu(x) j^A_\nu(0)|0\rangle = -g_{\mu\nu}\Pi_{A2}(q^2) + q_\mu q_\nu \Pi_A(q^2) \tag{25}$$

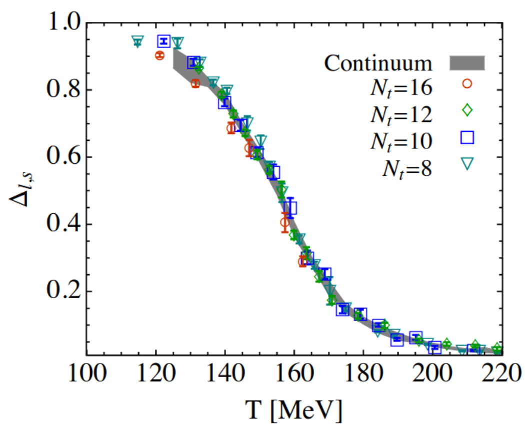

Fig. 2: Lattice calculation of subtracted chiral condensate which is defined as $\Delta_{l,s} = \frac{\langle\bar{\psi}\psi\rangle_{l,T} - \frac{m_l}{m_s}\langle\bar{\psi}\psi\rangle_{s,T}}{\langle\bar{\psi}\psi\rangle_{l,0} - \frac{m_l}{m_s}\langle\bar{\psi}\psi\rangle_{s,0}}$ with $l = u,d$ [9].

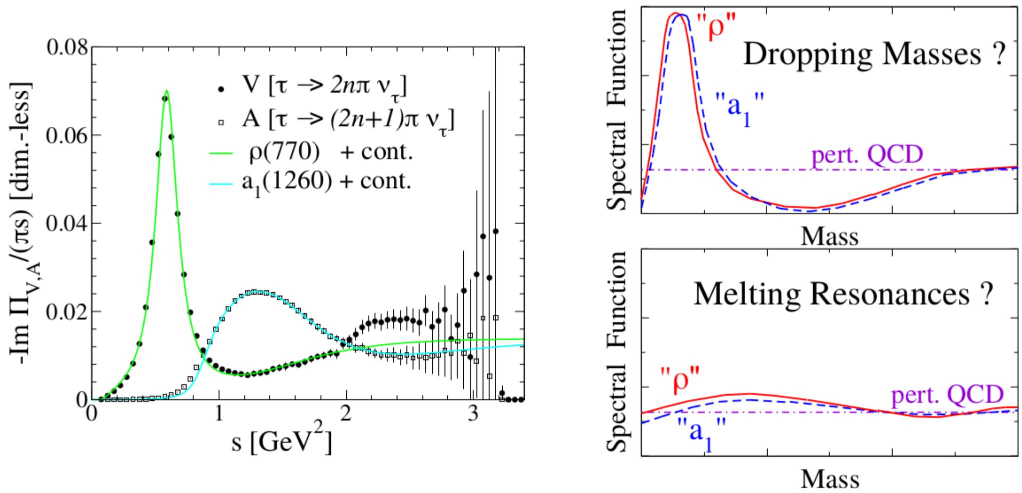

Fig. 3: On the left, the spectral functions in the axial and vector channel are shown which were extracted from hadronic τ decay data [12] including model fits supplemented by perturbative continua [13]. On the right, the two possible scenarios are shown, namely resonance melting and the dropping mass scenario [14].

Then if we assume that chiral symmetry is a symmetry of our theory and by exploiting the corresponding Ward identities and current algebra, it can be shown that [10][2]

$$\int_0^\infty ds \frac{1}{\pi}\{\mathrm{Im}\Pi_V(s) - \mathrm{Im}\Pi_A(s)\} = f_\pi^2 \tag{26}$$

With the well-known Gell-Mann-Oakes-Renner relation $m_\pi^2 f_\pi^2 = -2m_q\langle\psi\bar{\psi}\rangle$ we can write this as

$$\int_0^\infty ds \frac{1}{\pi}\{\mathrm{Im}\Pi_V(s) - \mathrm{Im}\Pi_A(s)\} = -2\frac{m_q}{m_\pi^2}\langle\psi\bar{\psi}\rangle \tag{27}$$

We can discuss two limits here. In the chiral limit where $m_q \to 0$ we obtain zero on the right-hand side. So, in the chiral limit the correlators seem to be equal to each other.
The other limit we can discuss is inserting eqn. 23 into 27 (or following the lattice QCD calculations for which $\langle\bar{\psi}\psi\rangle \xrightarrow{T\to\infty} 0$) which suggests that the correlators coincide at high temperatures. But this approach is too naive since eqn. 27 was derived at zero temperature.
A more careful analysis of the problem shows that [11]

$$\Pi_{V,A}(q,T) = (1-\varepsilon)\Pi_{V,A}(q,0) + \varepsilon\Pi_{A,V}(q,0) \tag{28}$$

with the mixing parameter $\varepsilon = \frac{T^2}{6f_\pi^2}$. At a finite temperature the correlators are not equal to each other but mix proportional to the square of the temperature.

One other interesting result Weinberg [10] found by pulling through his arguments is the relation $m_{a_1} = \sqrt{2}m_\rho$ which is in good agreement with experiment. This is not really a surprise, since we expect the a_1 and the ρ as resonances in the correlators in eqn. 25 and 24. If the correlators are equal to each other or at least mix under a (partially) restored chiral symmetry,

[2]Notice that I use a slightly different notation here. I use the Fourier transform of what Weinberg uses in his paper to make it easier to compare the results to experimental findings. Additionally, Weinberg chooses the normalization of his spectral function differently, i.e. his term before the spectral function is $\left(-g_{\mu\nu} + \frac{q_\mu q_\nu}{q^2}\right)$ whereas mine is $\left(-q^2 g_{\mu\nu} + q_\mu q_\nu\right)$ this gives an additional factor of s in the integral when we switch from his notation to the notation here.

so should also the resonances, i.e. the a_1 and the ρ.
There have been a lot of theoretical investigations which cover a lot of different outcomes depending on the model. There are the following possibilities [1]

1. The Weinberg sum rules imply the equality or at least the mixing of the axial and vector spectral functions if chiral symmetry is restored. This means that the spectral functions have a single peak at a single mass which could have basically any value. Chiral models prefer a value somewhere between the vacuum masses. If the spectral functions only mix there should be two resonances in the spectral functions with equal amplitude.

2. The other scenario would be the melting of the resonances because of the thermal broadening of the mesons in the thermalized medium – the QGP. This effect might be enhanced by the deconfinement which is expected to take place in a QGP along with chiral symmetry restoration. The both effects would melt the resonances.

Both scenarios are shown in fig. 3 alongside experimental data of the vacuum vector and axial spectral functions measured in hadronic τ decays.
The scenarios have also been investigated experimentally. Both the CERES experiment [15] and the NA60 experiment [16] reported that the broadening scenario for the ρ is more consistent with their data. They used ρ mesons decaying into dileptons which is a very clean probe since dileptons can be identified very precisely with a spectrometer. The spectral functions can also be theoretically related to the differential dilepton yield [14]

$$\frac{dN_{ll}}{d^4xd^4q} = -\frac{\alpha_{\text{em}}^2}{\pi^3 M^2} f^B(q_0;T)\frac{1}{3}g_{\mu\nu}\text{Im}\Pi_{\text{em}}^{\mu\nu}(M,q;\mu_B,T) \tag{29}$$

making dileptons a very interesting probe for vector mesons in the vacuum but also in strongly interacting media.

2 Data Analysis

2.1 Analysis Strategy

In the first section, we got a first insight on the importance of the a_1-ρ system as a probe for chiral symmetry restoration. Eventually, one would like to measure the a_1 in heavy-ion collisions decaying only into electromagnetically interacting particles so effects of the QGP would be visible. Since this is a feasibility study of the measurement of the a_1 in the ALICE detector we use the decay modes which can be most easily tracked with the detector. With its TPC the ALICE detector has a very precise tool to trace charged particles. The ALICE detector also offers three calorimeters, the PHOS, the EMCAL and the DCAL which can be used to measure the energy of neutral particles. Looking at table 1 what we want to do to analyse the a_1 in the $\pi^0\gamma$ channel, is to hope for the neutral pion to decay into two photons (which happens in approximately 99% of the cases [7]) and then measure them along with the other photon from the a_1 decay with the calorimeters. The other option is two hope for all of the photons to decay in the detector material and then use the dielectron pairs from the conversion to reconstruct the a_1. For the $\pi^0\pi^+\pi^-$ decay channel we can use the tracking capabilities of the TPC to trace the charged pions and then do the same procedure as for the other decay channel for the neutral pion.

Both techniques obviously have their advantages and disadvantages. The photon conversion method (PCM) works very well at low transverse momenta. This is because it uses the tracks of the charged particles to reconstruct the photon. Obviously the track of a particle with lower momentum will be bent more, i.e. have a smaller radius of curvature, then a particle with high momentum. Therefore a smaller radius of curvature should mean a better, i.e. smaller, resolution. We can estimate a resolution with $\sigma_{PCM} \sim R = \frac{p_T}{qB}$ by setting the centrifugal force of a particle equal to the Lorentz force in a magnetic field and assuming $p \simeq p_T$. For constant magnetic field and charge this estimate of the resolution obviously gets better with lower p_T. Another advantage is that particles can be identified relatively easily, e.g. using their specific energy loss in the TPC. One of the biggest disadvantages of PCM is the conversion probability. The conversion probability for ALICE for the integrated detector material for $R < 180$ cm and $|\eta| < 0.9$ is about 8.5% [17]. If we then have to take this to the power of three for the $\pi^0\gamma$ channel, this really dampens the already low probability to find the a_1 even more.

For the calorimeters we can also make a quick approximation of the resolution. If we assume Gaussian distribution of the response (variance scaling like $\sqrt{N}$ where N is the number of events) the relative resolution scales like $\frac{\sigma}{N} = \frac{\sqrt{N}}{N} = \frac{1}{\sqrt{N}}$. If we also assume that each photon carries some average energy $E \sim p_T$ in the calorimeter we get as an estimate $\sigma_{Calo} \sim \frac{1}{\sqrt{p_T}}$. This obviously gets better with high p_T. One disadvantage is that all the particles that make it past the other detectors will end up in the calorimeters which are located at the outermost radii of the whole apparatus. We also have to identify the particles which can be done by using first of all a

Particle	Decay Mode	Branching Ratio
a_1	$\pi^0\gamma$	$(0.15 \pm 0.07)\%$
a_1	$\pi^0\pi^+\pi^-$	seen, BR not known
ω	$\pi^0\gamma$	$(8.40 \pm 0.22)\%$
ω	$\pi^0\pi^+\pi^-$	$(89.3 \pm 0.06)\%$
η	$\pi^0\pi^+\pi^-$	$(22.92 \pm 0.28)\%$
ρ	$\pi^+\pi^-$	$\sim 100\%$

Table 1: Decay modes of the a_1 meson and control modes ω, η and ρ [7]

charged particle veto to get rid of all charged particles and then e.g. using the shower shape of the decaying particle in the calorimeter.
In table 1 there are also a few other particles shown which have the same decay modes as the a_1, the ω and the η and the ρ which should appear in the charged pion mass spectrum of the other decays. We can use these particle decays to see if our analysis is sensible.

2.2 $a_1 \to \pi_0\gamma$ analysis

2.2.1 Event Selection and Cuts

Event Selection
For the event selection we took all of the 13 TeV pp events into account which are flagged by the minimum bias INT7 trigger which requires a coinciding signal in the V0 detector arrays. We also required the detectors we used in the analysis to provide a good signal for the flagged events. Then we performed the basic pile-up rejection to get rid of events where several proton collisions happened in a too short time window for the single events to still be resolved. Finally, we required the z-coordinate of the primary vertex to be within 10 cm of the nominal interaction point and required the primary vertex to have at least one contributor. After this procedure about events where left.
Before the actual analysis starts, we already do some general cuts on all of the tracks that are found in the detector. They can be found in table 2 alongside the particle identification (PID) cuts which are used later in the analysis to identify the particles belonging to the tracks.

Track Cuts
The track p_T cut is used to reject the tracks for which the detector efficiency is low. Because the efficiency of the TPC drops significantly at around $p_T = 0.05$ GeV we used this value as the cut-off for the track p_T. The TPC cluster cut makes sure that at least 60% of the available clusters for the track are crossed to obtain a good signal. We also required all of the tracks to be refitted in the whole TPC. This assures good reconstruction of the tracks which is important to properly reconstruct the V^0 candidates which are candidates for photons in our analysis. Finally, we also reject particles with kinks. These are particles which decay weakly and therefore don't fit our event topology.
Then in the analysis we do a selection of all tracks based on their specific energy loss in the

Track Cut	Cut Range
track p_T	$p_T > 0.05$ GeV/c
TPC clusters	$\frac{N_{\text{TPC-Clusters}}}{N_{\text{findable TPC-Clusters}}} > 0.6$
require TPC refit	TRUE
rejection of tracks with kinks	TRUE
electron selection	$\lvert n\sigma_e\rvert < 3$
pion rejection	for $p < 0.4$ GeV/c: $n\sigma_\pi < 0.5$
	for $p > 0.4$ GeV/c: $n\sigma_\pi < 3$

Table 2: General track and PID cuts for electron candidates from photon conversions from the $a_1 \to \pi^0\gamma$ and subsequent $\pi^0 \to \gamma\gamma$ decay

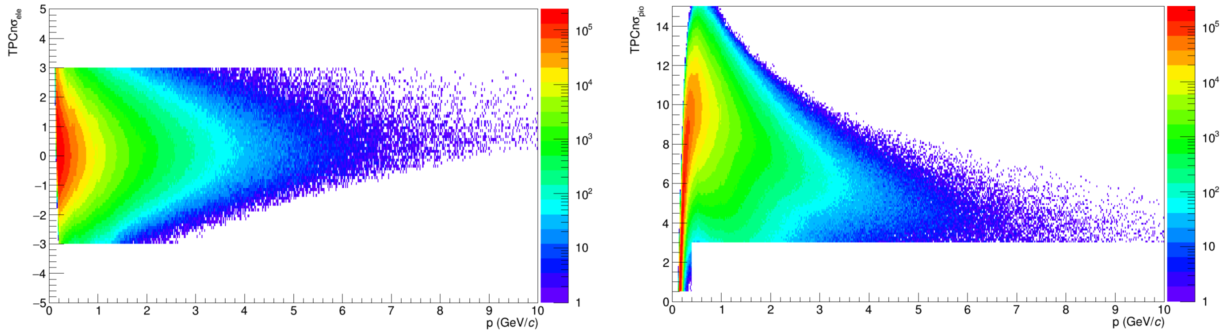

(a) $n\sigma_e$ versus p plot for the assumption of an electron

(b) $n\sigma_\pi$ versus p plot for the assumption of a pion

Fig. 4: The specific energy loss of the particles in the TPC expressed in terms of the $n\sigma$ discrimination variable plotted against the particle momentum, here only shown for the negative particles; the colour scale shows the number of counts

TPC. This is done using a discrimination variable $n\sigma_i$ which is defined as

$$n\sigma_i = \frac{S - \hat{S}_i}{\sigma_i} \tag{30}$$

The idea is to compare the measured signal S to the signal $\hat{S}_i$ which we expect assuming that the track comes from a certain particle species i. The difference is normalized by the expected signal resolution σ_i. If $n\sigma_i$ is close to zero, i.e. the signal is close to the expected signal, it is very likely that the particle we measured is the particle we used in our assumption to get the value of $n\sigma_i$ that is close to zero.
In the analysis we used the specific energy loss of the particles in the TPC as our signal. For the electrons we selected all tracks that lay within a 3σ band around the expected Bethe-Bloch line which seemed reasonable to reject most background. For the pions we have to differ two regions. For $p < 0.4$ GeV the Bethe-Bloch lines of the pions and electrons overlap, so we chose a stricter cut of $n\sigma_\pi < 0.5$ below $p = 0.4$ GeV to reject all candidates that looked like pions. For $p > 0.4$ GeV we used the same cut as for the electrons to reject the pions in this momentum region. Both times we also reject everything that lies below the theoretical pion Bethe-Bloch line to reject all particles that have an even bigger discrepancy than the pions. In figure 4 you can see $n\sigma$ for the assumption of an electron and a pion plotted against the momentum p after the cuts were applied.

V^0 cuts

quote and discuss cuts (see bachelor thesis for discussion which is basically the same, also add the other cuts which where not used and discuss why they were not used)

V0 cuts show helix cut, but no cut on helix radius

blablablablablabla

2.3 $a_1 \to \pi^0\pi^+\pi^-$ analysis

2.3.1 Cuts and Event Selection

quote and discuss cuts

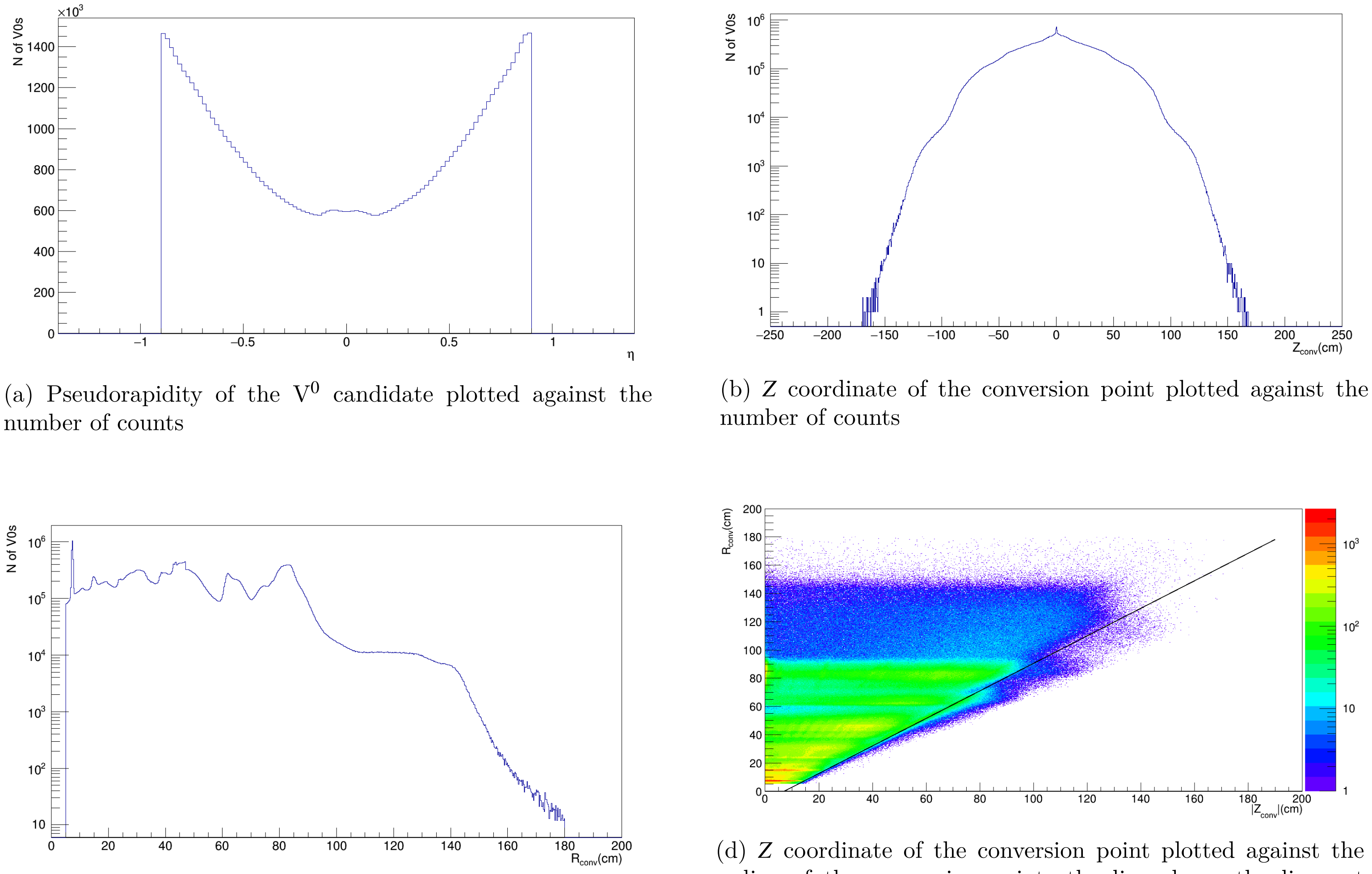

(a) Pseudorapidity of the V^0 candidate plotted against the number of counts

(b) Z coordinate of the conversion point plotted against the number of counts

(c) Radius of the conversion point plotted against the number of counts

(d) Z coordinate of the conversion point plotted against the radius of the conversion point; the line shows the line cut defined in table ?? and the colour scale shows the number of counts

Fig. 5: Plots of the geometric V^0 cuts as they were used in this analysis

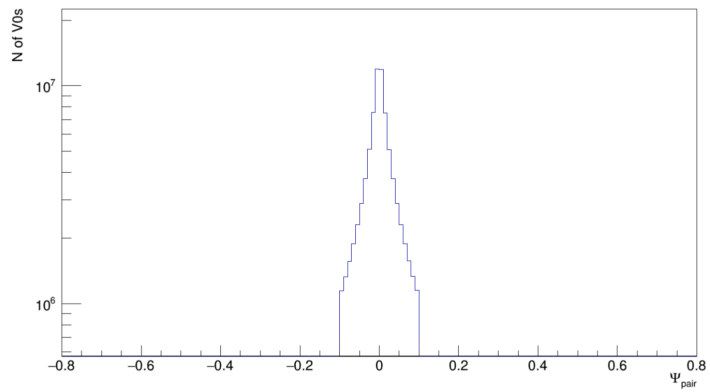

(a) Ψ_{pair} angle of the V^0 candidate plotted against the counts

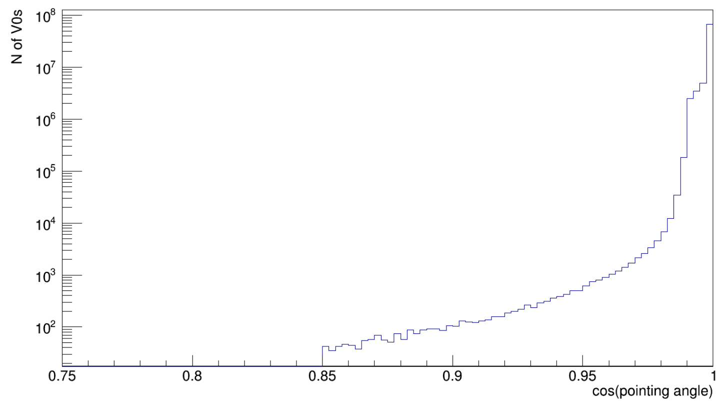

(b) cos(pointing angle) of the legs of the V^0 plotted against the counts

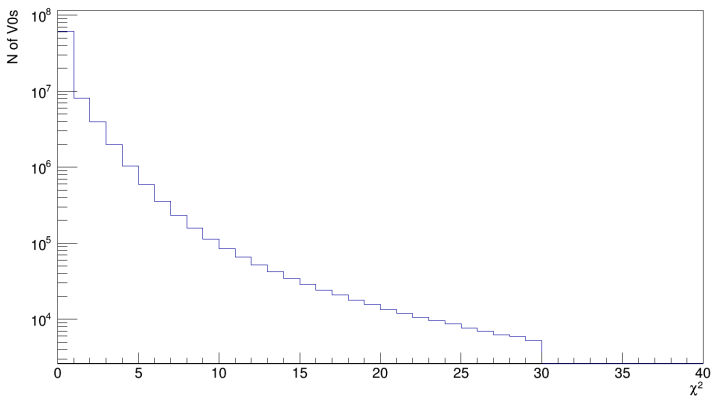

(c) χ^2 of the Kalman filtering method of tracks which form the V^0 plotted against the counts

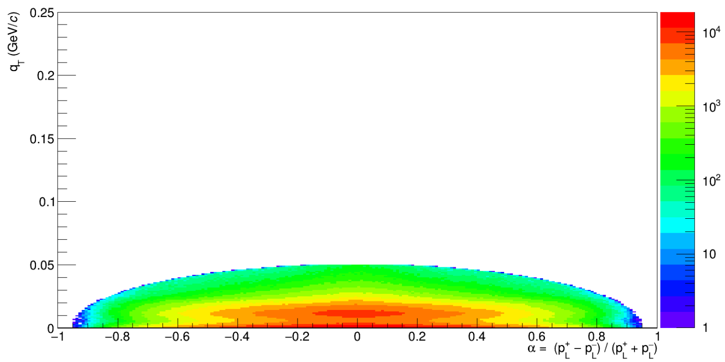

(d) Armenteros-Podolanski plot with the cut selecting the photons from the V^0 candidates

Fig. 6: Plots of the further V^0 cuts as they were used in this analysis

V^0 Cut	Cut Range
pseudorapidity of CP	$\lvert\eta_{\rm conv}\rvert < 0.9$
Z coordinate of CP	$\lvert Z_{\rm conv}\rvert < 240$ cm
radius of CP	5 cm $< \lvert R_{\rm conv}\rvert < 180$ cm
line cut	$R_{\rm conv} > \lvert Z_{\rm conv}\rvert \cdot f(\eta_{\rm max}) - Z_0$
	with $Z_0 = 7$ cm and $\eta_{\rm max} = 0.9$
$\Psi_{\rm pair}$ angle	$\lvert\Psi_{\rm pair}\rvert < 0.1$
cosine of pointing angle	$\cos(\text{pointing angle}) > 0.85$
χ^2 of Kalman filter	$\chi^2 < 30$
like-sign cut	reject V^0s with like-sign charged legs
elliptical cut in Armenteros-	$q_T < q_{T,\rm max} \cdot \sqrt{1-\alpha^2/\alpha^2_{\rm max}}$
Podolanski plot	with $q_{T,\rm max} = 0.05$ GeV/c, $\alpha_{\rm max} = 0.95$

Table 3: V^0 cuts used in the analysis; CP $\widehat{=}$ Conversion Point; $f(\eta_{\rm max})$ is defined in equation ??

ele track cuts: same as for other analysis

Track Cut	Cut Range
track p_T	$p_T > 0.05$ GeV/c
TPC clusters	$\frac{N_{\text{TPC-Clusters}}}{N_{\text{findable TPC-Clusters}}} > 0.6$
require TPC refit	TRUE
rejection of tracks with kinks	TRUE
electron selection	$\lvert n\sigma_e\rvert < 3$
pion rejection	for $p < 0.4$ GeV/c: $n\sigma_\pi < 0.5$
	for $p > 0.4$ GeV/c: $n\sigma_\pi < 3$

Table 4: General track and PID cuts for the electron candidates from photon conversions from the $\pi^0 \to \gamma\gamma$ decay

cuts on charged pions:

856 esdTrackCuts->SetRequireSigmaToVertex(kFALSE);

2.4 MC production

Track Cut	Cut Range
track p_T	$p_T > 0.05$ GeV/c
track pseudorapidity	$\|\eta\| < 0.8$
TPC clusters	$\frac{N_{\text{TPC-Clusters}}}{N_{\text{findable TPC-Clusters}}} > 0.8$
crossed TPC rows	$N_{\text{crossed rows}} > 70$
TPC cluster χ^2	$\frac{\chi^2}{N_{\text{clusters}}} < 4$
require TPC refit	TRUE
require ITS refit	TRUE
DCA to vertex p_T dependence χ^2	$0.0105 + \frac{0.0350}{p_T^{1.1}}$
DCA z-coord. to vertex χ^2	$z_{DCA} < 2$ cm
ITS cluster χ^2	$\frac{\chi^2}{N_{\text{clusters}}} < 36$
χ^2 constrained vs global track	$\chi^2 < 36$
rejection of tracks with kinks	TRUE
require sigma to vertex	FALSE
pion selection	$\|n\sigma_{\pi,TPC}\| < 3$
	$\|n\sigma_{\pi,TOF}\| < 3$

Table 5: General track and PID cuts for the pions from the $a_1 \rightarrow \pi^0\pi^+\pi^-$ decay

3 Results

show ρ peak which is by-product in charged pi-pi spectrum from 3pi a_1 channel. Try to properly fit with fitting script. might be difficult because of weird background, has already been measured in ALICE, e.g. [18].

4 Outlook

References

[1] Koch, Volker. Aspects of Chiral Symmetry. Int. J. Mod. Phys., E6:203–250, 1997.

[2] A. Bazavov, Tanmoy Bhattacharya, C. DeTar, H.-T. Ding, Steven Gottlieb, Rajan Gupta, P. Hegde, U. M. Heller, F. Karsch, E. Laermann, L. Levkova, Swagato Mukherjee, P. Petreczky, C. Schmidt, C. Schroeder, R. A. Soltz, W. Soeldner, R. Sugar, M. Wagner, and P. Vranas. Equation of state in $(2+1)$-flavor QCD. Phys. Rev. D, 90:094503, Nov 2014.

[3] Discussion of RHIC data leading to QGP discovery: BRAHMS collaboration (arXiv:nucl-ex/0410020), PHENIX collaboration (arXiv:nucl-ex/0410003), STAR collaboration (arXiv:nucl-ex/0501009), PHOBOS collaboration (arXiv:nucl-ex/0410022).

[4] LHC Experiments Committee. ALICE: Technical proposal for a large ion collider experiment at the CERN LHC. Technical report, ALICE collaboration, 12 1995.

[5] Berndt Müller, Jürgen Schukraft, and Bolesław Wysłouch. First Results from Pb+Pb Collisions at the LHC. Annual Review of Nuclear and Particle Science, 62(1):361–386, Nov 2012.

[6] Ellis, R.Keith and Stirling, W.James and Webber, B.R. QCD and Collider Physics, volume 8. Cambridge University Press, 2 2011.

[7] M. Tanabashi et al. Review of Particle Physics. Phys. Rev. D, 98:030001, Aug 2018.

[8] P. Gerber and H. Leutwyler. Hadrons Below the Chiral Phase Transition. Nucl. Phys. B, 321:387–429, 1989.

[9] Szabolcs Borsanyi, Zoltan Fodor, Christian Hoelbling, Sandor D Katz, Stefan Krieg, Claudia Ratti, and Kalman K. Szabo. Is there still any T_c mystery in lattice QCD? Results with physical masses in the continuum limit III. JHEP, 09:073, 2010.

[10] Steven Weinberg. Precise relations between the spectra of vector and axial vector mesons. Phys. Rev. Lett., 18:507–509, 1967.

[11] M. Dey, V. L. Eletsky, and B. L. Ioffe. Mixing of vector and axial mesons at finite temperature: an Indication towards chiral symmetry restoration. Phys. Lett., B252:620–624, 1990.

[12] R. Barate et al. Measurement of the spectral functions of axial - vector hadronic tau decays and determination of $\alpha_S(M^2(\tau))$. Eur. Phys. J. C, 4:409–431, 1998.

[13] Ralf Rapp. Dileptons in high-energy heavy ion collisions. Pramana, 60:675–686, 2003.

[14] R. Rapp, J. Wambach, and H. van Hees. The Chiral Restoration Transition of QCD and Low Mass Dileptons. Landolt-Bornstein, 23:134, 2010.

[15] D. Adamová et al. Modification of the ρ meson detected by low-mass electron–positron pairs in central PbAu collisions at 158 A GeV/c. Physics Letters B, 666(5):425–429, Sep 2008.

[16] J Seixas and the NA60 Collaboration. NA60 results on p_T spectra and the ρ spectral function in In–In collisions. Journal of Physics G: Nuclear and Particle Physics, 34(8):S1023–S1027, Jul 2007.

[17] ALICE Collaboration and others. Performance of the ALICE experiment at the CERN LHC. International Journal of Modern Physics A, 29(24):1430044, 2014.

[18] S. Acharya et al. Production of the $\rho^0(770)$ meson in pp and Pb-Pb collisions at $s_{NN} = 2.76$ TeV. Physical Review C, 99(6), Jun 2019.